Hybrid Switched-Inductor Converters for High Step-Up Conversion

Yu Tang, *Member, IEEE*, Dongjin Fu, Ting Wang, and Zhiwei Xu

***Abstract*—In applications where the high voltage gain is required, such as photovoltaic grid-connected system, fuel-cell and high-intensity discharge lamps for automobile, high step-up dc-dc converters have been introduced to boost the low voltage to a high bus voltage. The voltage gain of traditional boost converter is limited, considering the issues such as the system efficiency and current ripple. This paper proposes a class of hybrid switched-inductor converters (H-SLCs) for high step-up voltage gain conversion. First, the topological derivation of H-SLCs is deduced by combining the passive and active switched-inductor unit; second, this paper illustrates the operation modes of the proposed asymmetrical and symmetrical converters; third, the performance of the proposed converters is analyzed in detail and compared with existing converters; finally, a prototype is established in the laboratory, and the experimental results are given to verify the correctness of the analysis.**

***Index Terms*—DC/DC converter, high step-up, switched-inductor.**

I. Introduction

HIGH STEP-UP dc–dc converters have been developed in various applications, such as high-intensity discharge lamp ballasts for automobile headlamps, battery backup systems for uninterruptible power supplies, fuel-cell, and solar-cell power conditioning systems [1]–[3].

Fig. 1 presents the structure of a typical fuel-cell power plant [4]. Taking the cost and reliability issues into consideration, the voltage of the fuel-cell stack is usually lower than 40 Vdc; it is required to be boosted to a high voltage bus typically 180–200 Vdc for the dc/ac inverter. The maximum voltage ratio is approximate to ten times in this condition. The traditional boost converter cannot meet this requirement obviously, because the operated duty ratio of the switch in boost converter is close to 1 and induces high current ripple with low efficiency.

Various topologies have been developed to provide a high step-up without an extremely high duty ratio. The isolated converters can adjust the voltage ratio by increasing the turns ratio of the transformers [5]–[9]. The isolated voltage-type converters derived from the buck converter show high-input current ripple and high voltage stress across the secondary side diodes. The isolated current-type converters derived from the boost converter show inherent step-up capability, whereas the voltage spike across the switches caused by the leakage inductor should be carefully considered [10]–[12]. Moreover, the cost in isolated topologies is high with multistage dc/ac/dc power conversion and isolated sensors or controllers.

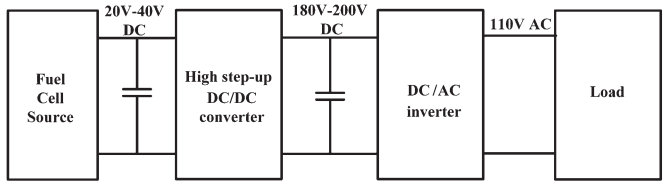

Fig. 1. Fuel-cell power plant with different power stages.

Nonisolated high step-up converters are employed to achieve high efficiency and low cost, and can be generalized as the coupled inductor type and noncoupled inductor type. A number of coupled inductor-based high step-up converters have been developed, by increasing the turns ratio of the coupled inductor, which is similar to that in isolated converters, high voltage gain can be achieved [13]–[16]. However, the leakage inductor of the coupled inductor is inevitable, which may cause high voltage spikes and add the voltage stress when the switch turns off [17], [18]. Various passive and active voltage clamping strategies have been developed with the cost of additional components [19]–[21]. By combining the conventional boost converter with the flyback converter, the outputs of the boost and flyback converters are in series to generate the high output voltage in the integrated boost–flyback converters [22]–[24]. Replacing the half-wave rectifier structure of the boost–flyback with bridge-doubler, the voltage conversional ratio can be extended. However, the voltage balance should be taken into consideration with the series structure.

The noncoupled inductor type can achieve high voltage gain with minimized magnetic components [25]–[28]. The cascade boost converters perform high voltage gain with a cascade structure, which show complex circuit and expensive cost. Although the two switches in the cascade boost converter can be integrated into one switch to reduce circuit complexity, the switch voltage and current stress are still high [26]–[28]. The number of capacitors and diodes also substantially increase along with the increase of the voltage gain ratio in the switched-capacitor-based converters. [28] presents a novel transformerless converter with high step-up voltage gain, the

Manuscript received May 9, 2013; revised October 23, 2013, February 1, 2014, May 15, 2014, and July 6, 2014; accepted July 31, 2014. Date of publication October 24, 2014; date of current version February 6, 2015. This work was supported by the Fundamental Research Funds for the Central Universities (NS2013037).

The authors are with the Jiangsu Key Laboratory of New Energy Generation and Power Conversion and the Jiangsu Province University Outstanding Science and Technology Innovation Team, Nanjing University of Aeronautics and Astronautics, Nanjing 210016, China (e-mail: ty8025@hotmail.com; fudongjin123@hotmail.com; wjslwt@hotmail.com; xuzwnuaa@hotmail.com).

Color versions of one or more of the figures in this paper are available online at http://ieeexplore.ieee.org.

Digital Object Identifier 10.1109/TIE.2014.2364797

0278-0046 © 2014 IEEE. Personal use is permitted, but republication/redistribution requires IEEE permission.
See http://www.ieee.org/publications_standards/publications/rights/index.html for more information.

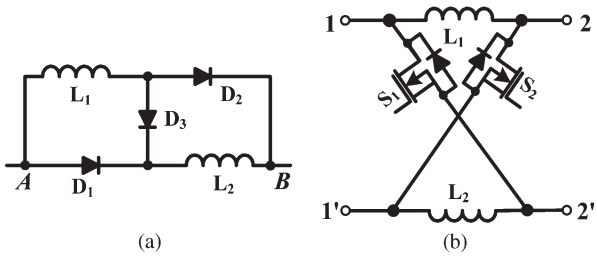

Fig. 2. Switched-inductor unit. (a) P-SL. (b) A-SL.

voltage stress and current stress on the power switches can be reduced; however, the voltage-conversion ratio is usually lower than 5.

Various switched-inductor and switched-capacitor structures to extend the voltage gain have been discussed in [29]. With the transition in series and parallel connection of the switched inductor, an inherent high voltage gain can be achieved. The switched-inductor-based boost converter is then derived, but the voltage gain is still limited and hard to deal with the ten times voltage ratio to meet the demands of the inverter; in addition, the switch voltage stress is also high. Although more switched cells can be added to increase the voltage conversion ratio, the topology is very complex.

This paper proposes a class of novel hybrid switched-inductor converters (H-SLCs) for high step-up conversion, which has the following advantages: high voltage-conversion ratio, low voltage stress across the switches, low conduction loss on switches, and easy to control. The operating principle and steady-state analysis of the H-SLCs with equal/different inductance are discussed in detail, and the experimental results are given to verify the analysis.

II. Topological Derivation of the H-SLC

Transformerless high-gain converters with passive switched-inductor (P-SL) unit and active switched-inductor (A-SL) unit have been presented in [29] and [28], respectively, as shown in Fig. 2.

The P-SL unit consists two inductors L_1, L_2 and three diodes D_1, D_2, D_3, when the potential voltage across the point A and B (i.e., V_{AB}) is positive, D_1, D_2 become conduct and D_3 is shutting off, two inductors are parallel connected; when V_{AB} becomes negative, D_1, D_2 are reverse biased and D_3 is conducted, then, the two inductors are series connected with the input (1-1') of the two-port network.

The A-SL unit is made up of two switches S_1, S_2 and two inductors L_1, L_2, the working principle of A-SL is similar to that of P-SL, when the switches S_1 and S_2 are turned on simultaneously, the inductors L_1 and L_2 are parallel connected; when S_1 and S_2 are turned off, L_1 and L_2 are series connected.

A high voltage gain can be achieved by combining the P-SL and A-SL units. The inductors L_1 and L_2 in A-SL unit can be substituted with P-SL unit, then the proposed H-SLCs can be obtained, as shown in Fig. 3, where Fig. 3(a) shows the asymmetrical structure, and Fig. 3(b) shows the symmetrical structure. The power switches share the same switching signals, which is easy to control. When the switches are conduct, the inductors operates in parallel connection and charged by the power source; when the switches are shutting off, the inductors operates in series connection and discharged to the output.

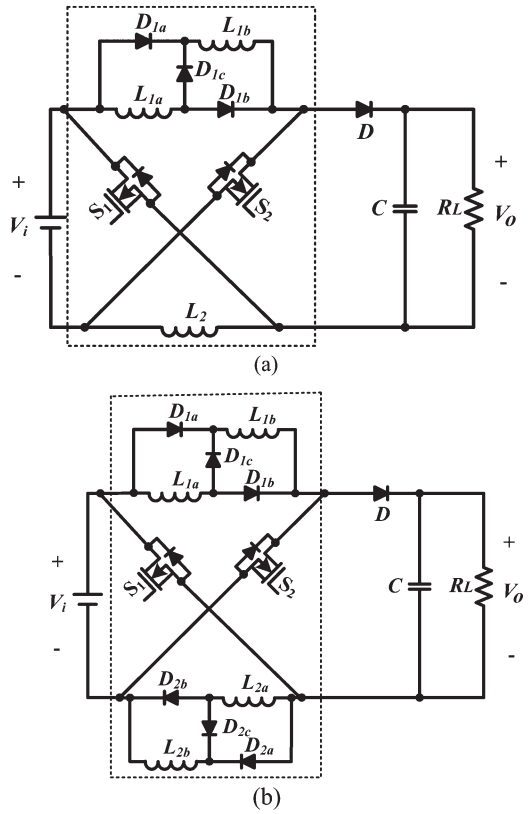

Fig. 3. Proposed H-SLC. (a) Asymmetrical structure. (b) Symmetrical structure.

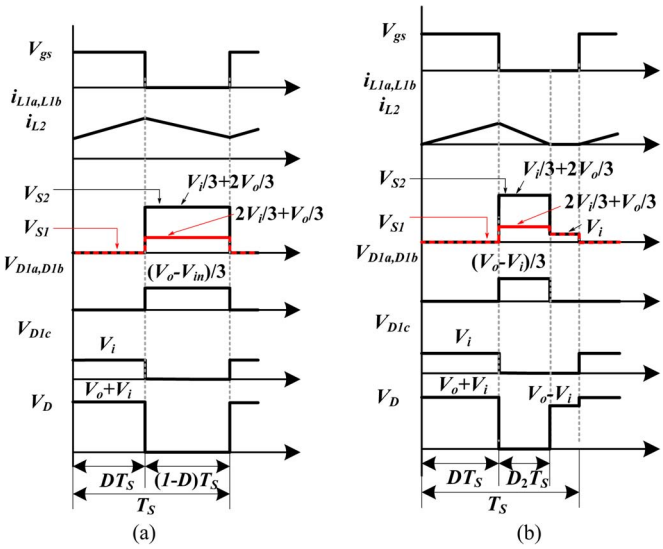

Fig. 4. Key waveforms of AH-SLC. (a) CCM. (b) DCM.

III. Operation Principle of Proposed Converters

A. Operating Modes of Asymmetrical Structure With an Equal Inductance

Fig. 4 illustrates the key waveforms of the proposed asymmetrical H-SLC (AH-SLC) in continuous-conduction mode

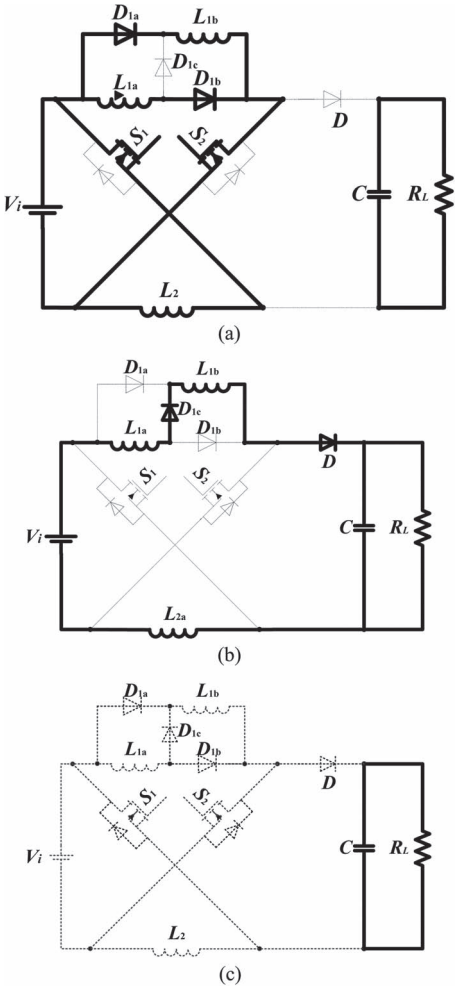

Fig. 5. Equivalent circuit in CCM and DCM operation of the AH-SLC.

(CCM) operation and discontinuous-conduction mode (DCM) operation. The equivalent circuit in CCM operation is shown in Fig. 5(a) and (b).

1) Mode 1 $[t_0 - t_1]$: The switches S_1 and S_2 are turned on during this time interval. The equivalent circuit is shown in Fig. 5(a). The three inductors L_{1a}, L_{1b}, L_2 are charged in parallel by the power source. The voltage across the inductors can be expressed as

$$V_{L1a} = V_{L1b} = V_{L2} = V_i. \tag{1}$$

2) Mode 2 $[t_1 - t_2]$: During this time interval, S_1 and S_2 are turned off. The equivalent circuit is shown in Fig. 5(b). The three inductors L_{1a}, L_{1b}, L_2 are series connected to transfer the energy to output. The voltage across the inductors is

$$V_{L1a} = V_{L1b} = V_{L2} = \frac{V_i - V_o}{3}. \tag{2}$$

Based on the voltage–second balancing of inductors, the following equation can be derived:

$$D \cdot V_i + (1 - D) \cdot \frac{V_i - V_o}{3} = 0. \tag{3}$$

The voltage gain in CCM operation is

$$G_{\mathrm{CCM}} = \frac{V_o}{V_i} = \frac{1 + 2D}{1 - D}. \tag{4}$$

The equivalent circuit in DCM operation is shown in Fig. 5(a)–(c).

1) Mode 1 $[t_0 - t_1]$: This mode is similar to Mode 1 in CCM operation. During the time t_1, the peak current through the inductors L_{1a}, L_{1b}, L_2 is

$$i_{L1ap} = i_{L1bp} = i_{L2a} = \frac{V_i}{L} D T_S \tag{5}$$

where $L_{1a} = L_{1b} = L_2 = L$.

2) Mode 2 $[t_1 - t_2]$: This mode is similar to Mode 2 in CCM operation. During time t_2, the inductor current decreased to 0. i_{L1ap}, i_{L1bp}, i_{L2a} can be expressed as

$$i_{L1ap} = i_{L1bp} = i_{L2a} = \frac{V_o - V_i}{3L} D_2 T_S. \tag{6}$$

3) Mode 3 $[t_2 - t_3]$: During this time interval, the equivalent circuit is shown in Fig. 5(c). The load is supplied by the capacitor. Combining (5) and (6), the relationship between D_2 and D is

$$D_2 = \frac{3V_i}{V_o - V_i} D. \tag{7}$$

The average current through the output diode is equal to load current I_o; therefore,

$$\frac{1}{2} D_2 i_{L1p} = I_o = \frac{V_o}{R_L}. \tag{8}$$

Combining (5), (7), and (8), we can derive

$$V_o = \frac{1 + \sqrt{1 + \frac{6D^2}{\tau}}}{2} V_i. \tag{9}$$

The time constant τ is defined as

$$\tau = \frac{L f_S}{R_L} \tag{10}$$

where L is the inductance of the three inductors; f_S is the switching frequency; R_L is the load.

The voltage gain in DCM operation is

$$G_{\mathrm{DCM}} = \frac{V_o}{V_i} = \frac{1 + \sqrt{1 + \frac{6D^2}{\tau}}}{2}. \tag{11}$$

B. Operating Modes of Symmetrical Structure With an Equal Inductance

Fig. 6 shows the key waveforms of the proposed symmetrical H-SLC (SH-SLC) in CCM operation and DCM operation. The equivalent circuit in CCM operation is shown in Fig. 7(a) and (b).

1) Mode 1 $[t_0 - t_1]$: During this time interval, S_1 and S_2 are turned on. The current-flow path is shown in Fig. 7(a). The four inductors L_{1a}, L_{1b}, L_{2a}, L_{2b} are charged by the

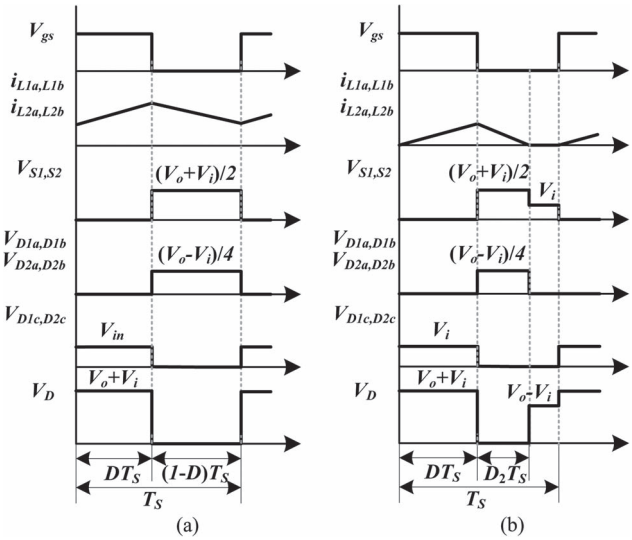

Fig. 6. Key waveforms of SH-SLC. (a) CCM. (b) DCM.

power source in parallel. The voltage across the inductors can be expressed as

$$V_{L1a} = V_{L1b} = V_{L2a} = V_{L2b} = V_i. \tag{12}$$

2) Mode 2 $[t_1 - t_2]$: During this time interval, S_1 and S_2 are turned off. The current-flow path is shown in Fig. 7(b). The four inductors L_{1a}, L_{1b}, L_{2a}, L_{2b} are discharged to the output in series. The voltage across the inductors is

$$V_{L1a} = V_{L1b} = V_{L2a} = V_{L2b} = \frac{V_i - V_o}{4}. \tag{13}$$

Based on the voltage–second balancing of inductors, we can derive

$$D \cdot V_i + (1 - D) \cdot \frac{V_i - V_o}{4} = 0. \tag{14}$$

The voltage gain in CCM operation is

$$G_{\mathrm{CCM}} = \frac{V_o}{V_i} = \frac{1 + 3D}{1 - D}. \tag{15}$$

The equivalent circuit in DCM operation is shown in Fig. 7(a)–(c).

1) Mode 1 $[t_0 - t_1]$: This mode is similar to Mode 1 in CCM operation. During time t_1, the peak current i_L through the inductors L_{1a}, L_{1b}, L_{2a}, L_{2b} is

$$i_{L1ap} = i_{L1bp} = i_{L2ap} = i_{L2bp} = \frac{V_i}{L} DT_S \tag{16}$$

where $L_{1a} = L_{1b} = L_{2a} = L_{2b} = L$.

2) Mode 2 $[t_1 - t_2]$: This mode is similar to Mode 2 in CCM operation. During time t_2, the inductor current decreased to 0. i_{L1ap}, i_{L1bp}, i_{L2ap}, i_{L2bp} can be expressed as

$$i_{L1ap} = i_{L1bp} = i_{L2ap} = i_{L2bp} = \frac{V_o - V_i}{4L} D_2 T_S. \tag{17}$$

3) Mode 3 $[t_2 - t_3]$: During this time interval, the equivalent circuit is shown in Fig. 5(c). The load is supplied by

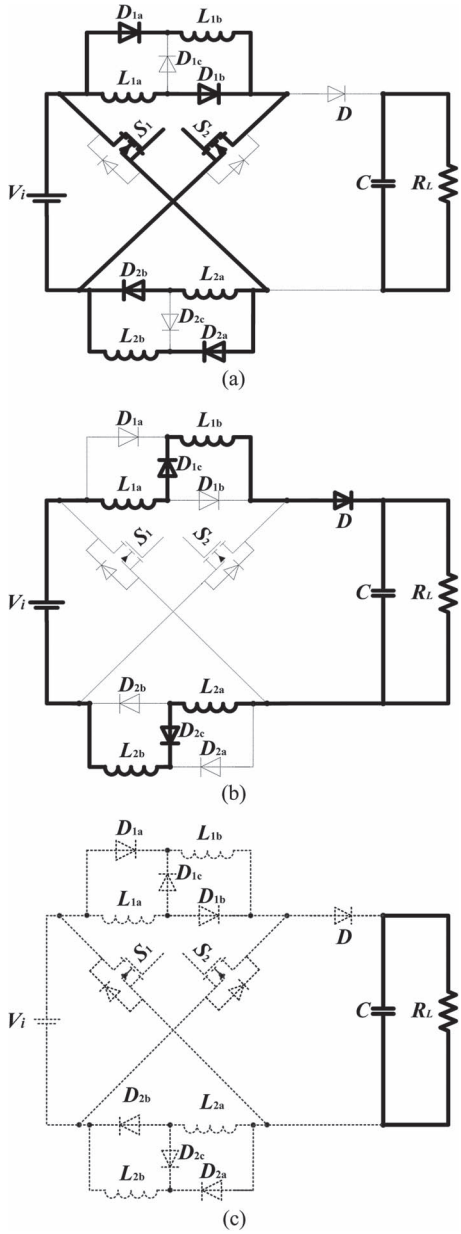

Fig. 7. Equivalent circuit of SH-SLC in CCM and DCM.

the capacitor. Combining (16) and (17), D_2 could be expressed as

$$D_2 = \frac{4V_i}{V_o - V_i} D. \tag{18}$$

The average current through the output diode is equal to load current I_o; therefore,

$$\frac{1}{2} D_2 i_{L1p} = I_o = \frac{V_o}{R_L}. \tag{19}$$

Combining (16), (18) and (19), the output voltage can be obtained

$$V_o = \left(\frac{1}{2} + \frac{1}{2} \sqrt{1 + \frac{8D^2}{\tau}} \right) V_i. \tag{20}$$

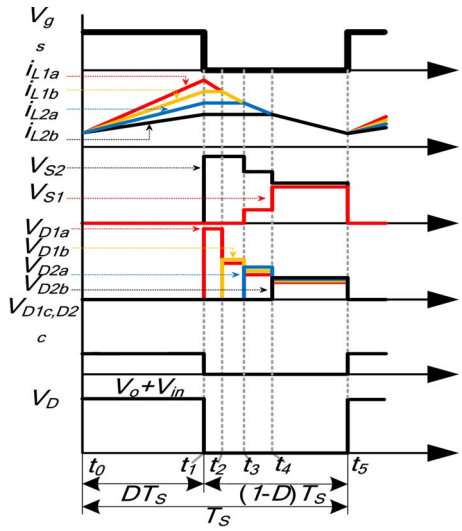

Fig. 8. Key waveforms with different inductance.

The voltage gain in DCM operation is

$$G_{\mathrm{DCM}} = \frac{V_o}{V_i} = \frac{1}{2} + \frac{1}{2}\sqrt{1 + \frac{8D^2}{\tau}}. \tag{21}$$

C. Operating Modes With Different Inductance

Assuming the inductance of the inductors is unequal, the operating modes of the converter are quite different with the situation when the inductance is equal.

The following analysis is given on SH-SLC as an example, the operation principles of AH-SLC is similar.

The CCM operation of SH-SLC is analyzed in the following. The possible situations are too excessive to analyze, in order to simplify the analysis, assuming the ordering of the inductance is $L_{1a} < L_{1b} < L_{2a} < L_{2b}$. The key waveforms in CCM operation is shown in Fig. 8. The equivalent circuit is given in Fig. 9.

1) Mode 1$[t_0 - t_1]$: During this time interval, S_1 and S_2 are turned on. The equivalent circuit is shown in Fig. 9(a). The four inductors are charged in parallel by the power source. The voltage across the inductors can be expressed with equation (12).
2) Mode 2 $[t_1 - t_2]$: During this time interval, S_1 and S_2 are turned off. The equivalent circuit is shown in Fig. 9(b). The inductors L_{1b}, L_{2a}, L_{2b} are short-circuited. L_{1a} is discharged to output. i_{L1a} decreased with the rate $(V_o - V_i)/L_{1a}$ and i_{L1b}, i_{L2a}, i_{L2b} remain unchanged. The voltage across the inductors is

$$\begin{cases} V_{L1a} = V_i - V_o \\ V_{L1b} = V_{L2a} = V_{L2b} = 0 \end{cases}. \tag{22}$$

3) Mode 3 $[t_2 - t_3]$: During this time interval, S_1 and S_2 are turned off. The equivalent circuit is shown in Fig. 9(c). During the time t_2, $i_{L1a}(t_2) = i_{L1b}(t_2)$, D_{1b} is reverse-biased, The inductors L_{2a}, L_{2b} are short-circuited. L_{1a} and L_{1b} are series connected and transfer the energy

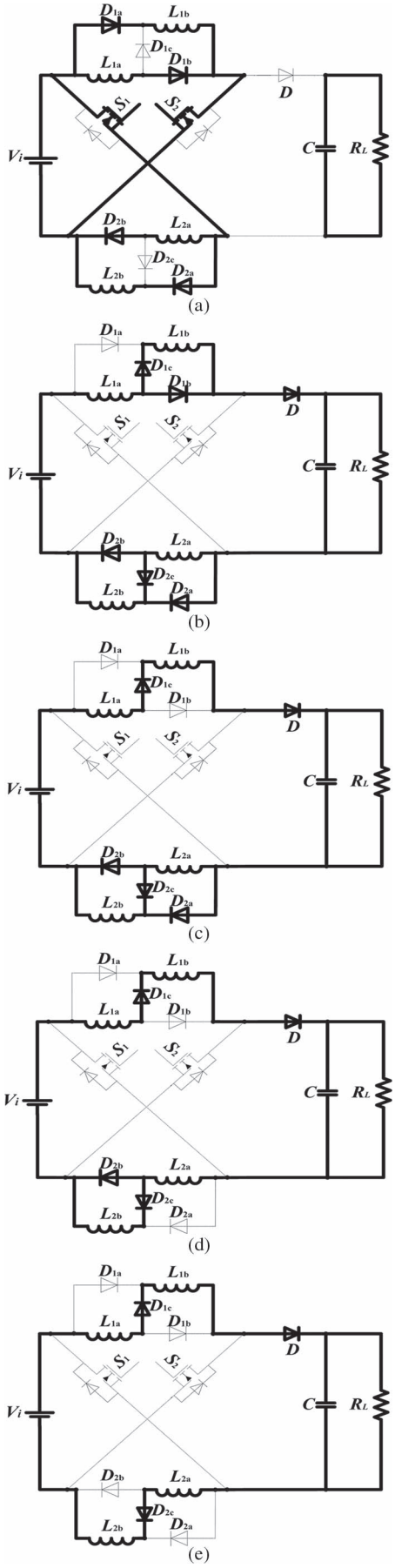

Fig. 9. Equivalent circuit of SH-SLC with different inductance.

to output. i_{L1a}, i_{L1b} is decreased with the rate $(V_o - V_i)/(L_{1a} + L_{1b})$ and i_{L2a}, i_{L2b} remain unchanged. The voltage across the inductors is

$$\begin{cases} V_{L1a} = \frac{L_{1a}}{L_{1a}+L_{1b}}(V_i - V_o) \\ V_{L1b} = \frac{L_{1b}}{L_{1a}+L_{1b}}(V_i - V_o) \\ V_{L2a} = V_{L2b} = 0. \end{cases} \tag{23}$$

4) Mode 4 $[t_3 - t_4]$: During this time interval, S_1 and S_2 are turned off. The equivalent circuit is shown in Fig. 9(d). During the time t_3, $i_{L1a}(t_3) = i_{L1b}(t_3) = i_{L2a}(t_3)$, D_{2a} is reverse-biased, The inductor L_{2b} is short-circuited. L_{1a}, L_{1b}, L_{2a} are series connected and transfer the energy to output. i_{L1a}, i_{L1b}, i_{L2a} is decreased with the rate $(V_o - V_i)/(L_{1a} + L_{1b} + L_{2a})$ and i_{L2b} remains unchanged. The voltage across the inductors is

$$\begin{cases} V_{L1a} = \frac{L_{1a}}{L_{1a}+L_{1b}+L_{2a}}(V_i - V_o) \\ V_{L1b} = \frac{L_{1b}}{L_{1a}+L_{1b}+L_{2a}}(V_i - V_o) \\ V_{L2a} = \frac{L_{2a}}{L_{1a}+L_{1b}+L_{2a}}(V_i - V_o) \\ V_{L2b} = 0. \end{cases} \tag{24}$$

5) Mode 5 $[t_4 - t_5]$: During this time interval, S_1 and S_2 are turned off. The current-flow path is shown in Fig. 9(e). During the time t_4, $i_{L1a}(t_4) = i_{L1b}(t_4) = i_{L2a}(t_4) = i_{L2b}(t_4)$, D_{2b} is reverse-biased. L_{1a}, L_{1b}, L_{2a}, L_{2b} are series connected and discharged to output. i_{L1a}, i_{L1b}, i_{L2a}, i_{L2b} is decreased with the rate $(V_o - V_i)/(L_{1a} + L_{1b} + L_{2a} + L_{2b})$. The voltage across the inductors is

$$\begin{cases} V_{L1a} = \frac{L_{1a}}{L_{1a}+L_{1b}+L_{2a}+L_{2b}}(V_i - V_o) \\ V_{L1b} = \frac{L_{1b}}{L_{1a}+L_{1b}+L_{2a}+L_{2b}}(V_i - V_o) \\ V_{L2a} = \frac{L_{2a}}{L_{1a}+L_{1b}+L_{2a}+L_{2b}}(V_i - V_o) \\ V_{L2b} = \frac{L_{2b}}{L_{1a}+L_{1b}+L_{2a}+L_{2b}}(V_i - V_o). \end{cases} \tag{25}$$

Based on the voltage–second balancing of inductors, combining the equations (12), (22)–(25), the voltage gain in CCM operation with different inductance is

$$G'_{\mathrm{CCM}} = \frac{V_o}{V_i} = \frac{1+3D}{1-D}. \tag{26}$$

Compared with (15), the voltage gain is the same.

IV. Analysis of the Proposed Converter

The voltage gain of AH-SLC is smaller than SH-SLC and presents asymmetrical stress across the devices. Considering the system design simplicity, the symmetrical topology is preferred.

The voltage stress of switches and diodes is increased with different inductance operation; therefore, the operation with equal inductors is preferred. The following analysis is given with equal inductance.

A. External Characteristic of SH-SLC

When operated in boundary conduction mode operation, the voltage gain in CCM is equal to DCM. Combining (15) and (21), the boundary normalized inductor time constant can be derived as follows:

$$\tau_B = \frac{D(1-D)^2}{2(1+3D)}. \tag{27}$$

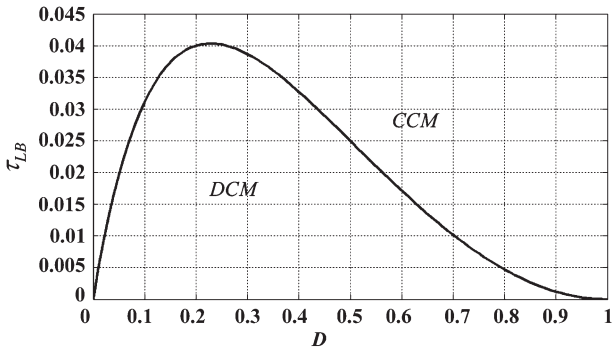

Fig. 10. Boundary condition of the converter.

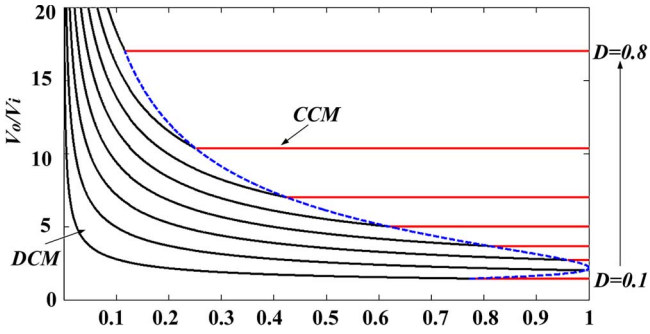

Fig. 11. External characteristic of the converter.

The relationship of τ_B and D is shown in Fig. 10. When $\tau > \tau_B$, the converter operates in CCM; when $\tau < \tau_B$, the converter operates in DCM.

In DCM operation, the critical load current is

$$I_{oG} = \frac{1}{2}(1-D)I_{L\max} = \frac{1}{2}(1-D)\Delta I_L = \frac{1}{2}\frac{V_i}{Lf_s}D. \tag{28}$$

Combining (15), we can derive

$$I_{oG} = \frac{D\frac{(1-D)^2}{1+3D}}{2Lf_s}V_o. \tag{29}$$

I_{oG} reaches its maximum value when $D = 0.2287$

$$I_{oG\max} = 0.0403\frac{V_o}{Lf_s}. \tag{30}$$

Fig. 11 shows the external characteristic of the converter. The dashed line shows the boundary of the CCM and DCM.

B. Voltage Gain

The voltage gain of the proposed AH-SLC and SH-SLC is given in Fig. 12 and compared with the existing boost converter, the switched-inductor boost converter (SL-Boost), and the switched-capacitor boost converter (SC-Boost).

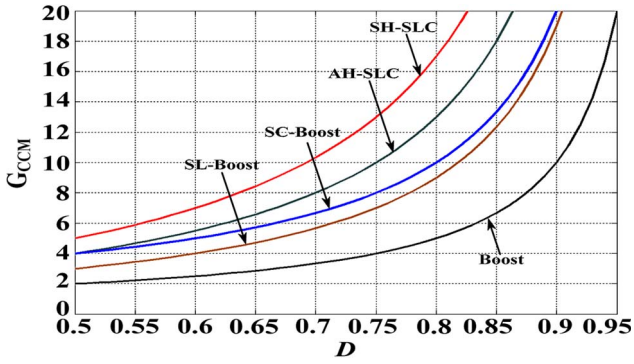

Fig. 12. Comparison of voltage gain.

TABLE I
PERFORMANCE BETWEEN DIFFERENT CONVERTERS

	SH-SLC	AH-SLC	SC-Boost	SL-Boost	Boost
Voltage gain	$\frac{1+3D}{1-D}$	$\frac{1+2D}{1-D}$	$\frac{2}{1-D}$	$\frac{1+D}{1-D}$	$\frac{1}{1-D}$
Voltage of MOSFET	$\frac{(1+G)Vi}{2}$	$\frac{1+2GVi}{3}$ $\frac{2+GVi}{3}$	$\frac{GVi}{2}$	GVi	GVi
Voltage of output diodes	$(1+G)Vi$	$(1+G)Vi$	$\frac{GVi}{2}$	GVi	GVi
Voltage of diodes in the P-SL	$\frac{(G-1)V_i}{4}$ Vi	$\frac{(G-1)V_i}{3}$ Vi		$\frac{(G-1)Vi}{2}$ Vi	
Voltage of diodes in the SC			$\frac{GVi}{2}$		
I_L/I_O	$\frac{G_{CCM}+3}{4}$		G_{CCM}	$\frac{G_{CCM}+1}{2}$	G_{CCM}

The expressions of the voltage gain in an ideal situation (i.e., the equivalent series resister of the device and the voltage drop of the diodes are ignored) are shown in Table I.

All the five converters are noncoupled inductor-type topologies. As can be seen, high voltage gain can be achieved in the proposed converter, and the ten times voltage ratio can be desired when $D = 0.7$, thus can reduce the current ripple and current stress of power components efficiently.

C. Voltage Stress

During the ON-state of the SH-SLC under CCM operation, the voltage across the diode D_{1c}, D_{2c}, and D can be expressed as

$$\begin{cases} V_{D1c} = V_{D2c} = V_i \\ V_D = V_o + V_i. \end{cases} \tag{31}$$

During the OFF-state of the SH-SLC under CCM operation, the voltage across the diode D_{1a}, D_{1b}, D_{2a}, D_{2b} and switches

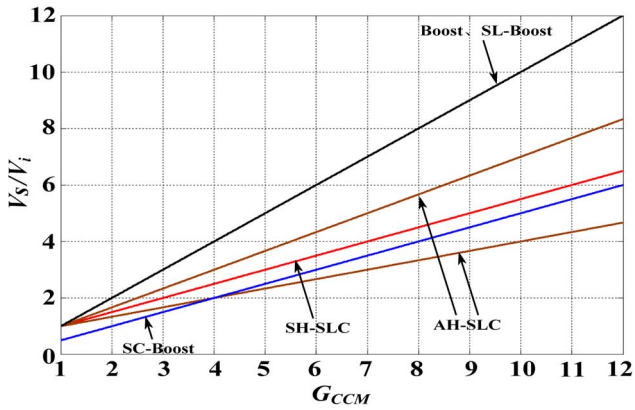

Fig. 13. Comparison of voltage stress.

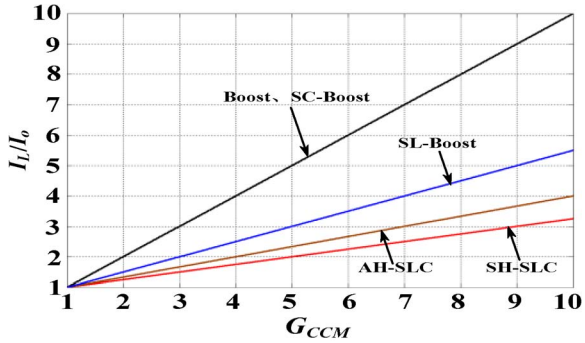

Fig. 14. Comparison of average inductor current.

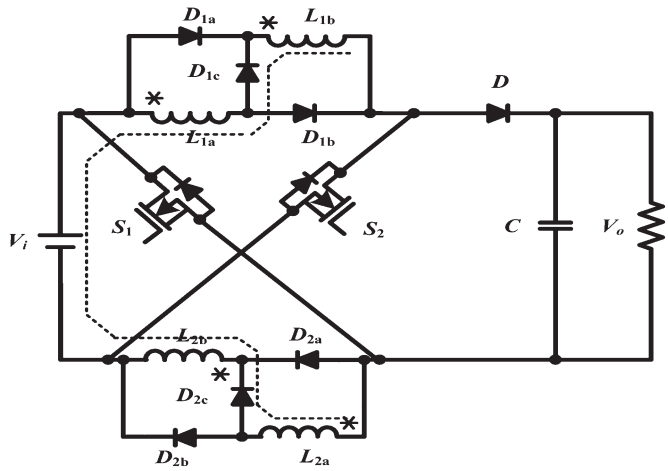

Fig. 15. Magnetic components integration.

S_1, S_2 can be expressed as

$$\begin{cases} V_{D1a} = V_{D1b} = V_{D2a} = V_{D2b} = \frac{V_o - V_i}{4} \\ V_{S1} = V_{S2} = \frac{V_o + V_i}{2}. \end{cases} \tag{32}$$

Table I shows the voltage stress across the power devices of the five converters in CCM operation mode.

The comparison of switch voltage stress in the four converters is shown in Fig. 13. To realize the same voltage ratio, the boost converter and the SL-Boost converter present the high voltage stress across the switch; whereas the switch voltage stress is greatly decreased in SH-SLC and SC-Boost. That

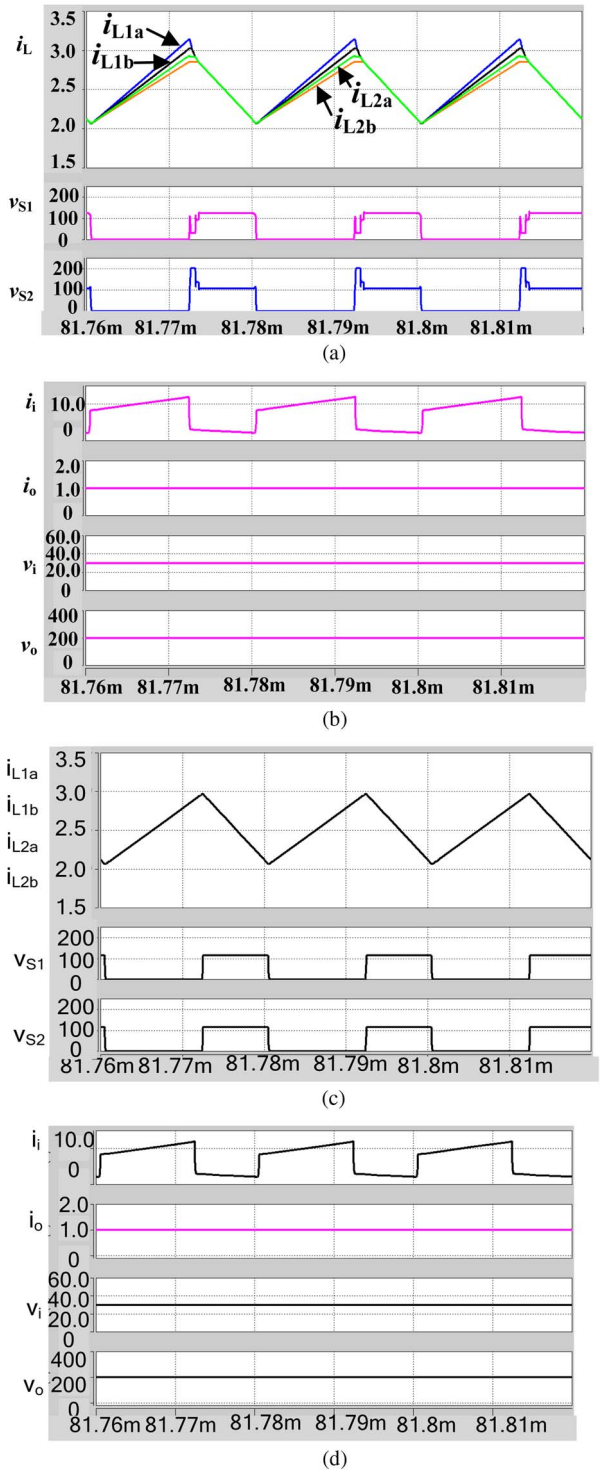

Fig. 16. Simulation results.

means the switches with low voltage stress can be utilized, which is beneficial to the efficiency and cost.

D. Inductor Current

The average inductor current of the five converters are shown in Table I, and we can see the difference from Fig. 14 clearly and simple.

The peak current of the inductor can be expressed as

$$I_{\text{peak-L}} = (1 + K_i)I_L \propto I_L \tag{33}$$

TABLE II
UTILIZED COMPONENTS AND PARAMETERS OF SH-SLC

Components	Parameters
V_{in}(input voltage)	20-40V
V_o(output voltage)	200V
P_o(maximum output power)	200W
f_s(switching frequency)	50kHz
L_{1a}, L_{1b}, L_{2a},L_{2b}(inductors)	500uH
S_1,S_2(Power MOSFET)	IRF360
D_{1a}, D_{1b}, D_{2a}, D_{2b} (Diodes)	EGP20B
D_{1c}, D_{2c} (Diodes)	EGP50B
D (Output Diodes)	SF26
C (Output capacitor)	470uF/250V

where K_i is the factor of the current ripple, assuming all the topologies share the same K_i, the peak current through the inductor is proportional to the average inductor current I_L. Thus, the peak current through the inductor can be presented by I_L.

E. Magnetic Components Integration Consideration

In fact, all the inductors of the proposed topology with equal inductance share the same operation condition. As shown in Fig. 15, the inductors can be integrated into one magnetic core, which helps to reduce the size of magnetic components.

V. Simulation Verification

Fig. 16 illustrated the simulation results of the inductors and power switches with different inductance [shown in Fig. 16(a) and (b)] and with the same inductance [as Fig. 16(c) and (d)].

As shown in Fig. 16, different inductance may increase the voltage stress on the power MOSFET, which would decrease the efficiency.

VI. Experimental Verification

In order to verify the effectiveness of the analysis, a SH-SLC prototype is built and tested in the laboratory. As Section IV shown, the different inductance would increase the voltage stress on the switches. Thus, the main components and parameters are summarized in Table II.

Fig. 17 shows the waveforms with 20 V input. Fig. 17(a) shows the switching signal V_{gs1} and V_{gs2}, the voltage V_{ds1} and V_{ds2}. Fig. 17(b) shows switching signal V_{gs} and inductor current of L_{1a}, L_{1b}. When the switches are on, the inductor current increases; when the switches are off, the inductor current decreases. The calculated inductor current is 3.25 A, which is approximate to the experimental results. Fig. 17(c) shows the diode voltage V_{D1a}, V_{D1b}. Fig. 17(d) shows the diode voltage V_D, V_{D1c}. Fig. 17(e) shows the input voltage V_i and output voltage V_o and the input current I_{in}.

Fig. 18 shows the waveforms of V_{gs}, V_{ds1}, V_{ds2} with 30-V input. Fig. 19 shows the same waveforms with 40-V input. As shown in Figs. 17–19, the voltage stresses on switches are $(V_i + V_o)/2$. Fig. 20 shows the efficiency of the proposed converter under $V_i = 20{-}40$ V, $V_o = 200$ V, $P_o = 50{-}200$ W. As can be seen, the efficiency is higher with the increase of input voltage. Fig. 21 shows the prototype.

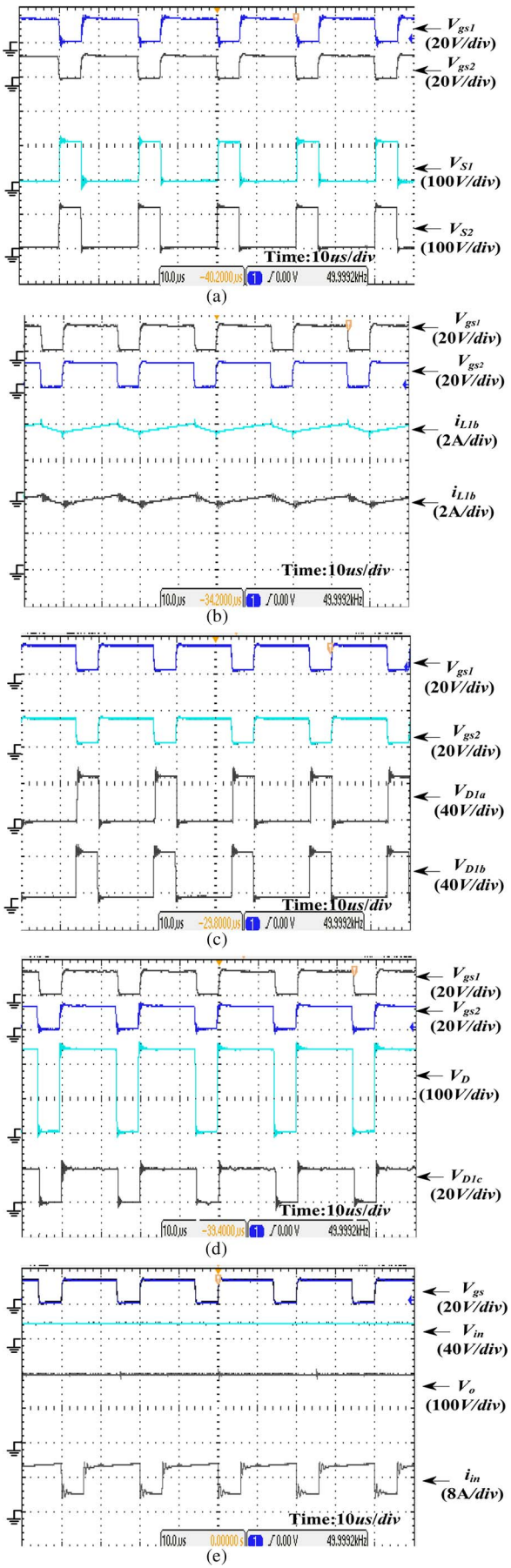

Fig. 17. Experimental waveforms when $V_i = 20$.

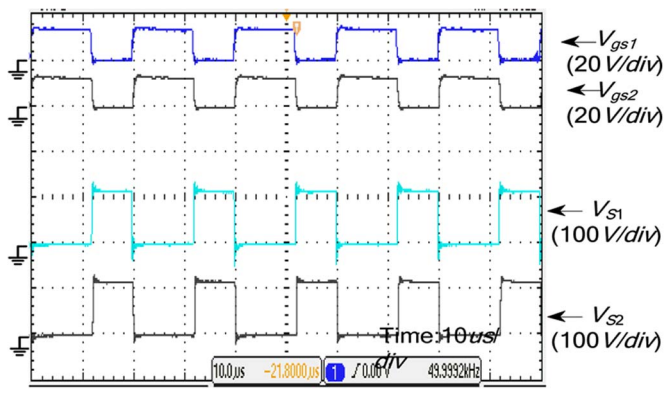

Fig. 18. Experimental waveforms when $V_i = 30$ V.

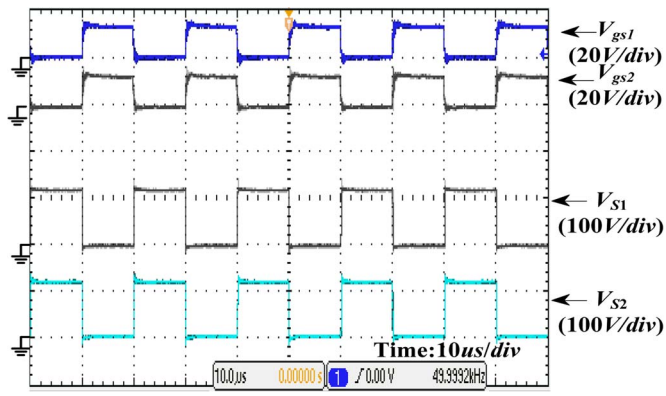

Fig. 19. Experimental waveforms when $V_i = 40$ V.

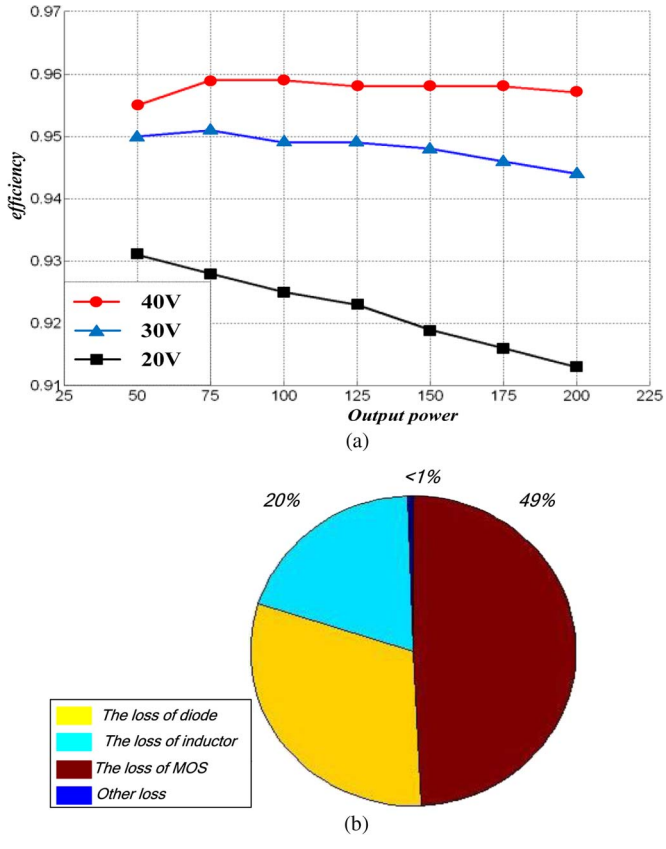

Fig. 20. Efficiency curve and proportion of loss.

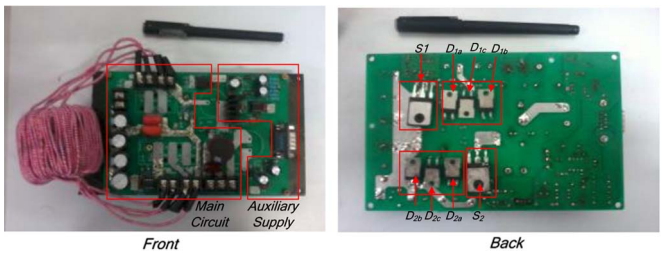

Fig. 21. Prototype board.

Fig. 20(a) shows the experimental efficiency curve of the proposed converter and (b) shows the proportion of different losses when $V_i = 20$ V $V_o = 200$ V $P_o = 200$ W.

VII. Conclusion

This paper has studied the H-SLCs, which are based on the switched-inductor cell and active-network. The following are the characteristics of the converters.

1) The proposed converter can achieve a high gain (up to ten times) with a small duty cycle that is difficult for traditional boost converter.
2) The proposed SH-SLC combines the advantages of a switched-inductor cell that can reduce the current stress of inductors and active-network, which can bring down the voltage stress of switches.
3) The inductors in the SL-cell can be integrated into one magnetic core, which helps to reduce the size of magnetic components.
4) Simulation and experimental results have been given to verify the analysis.

References

[1] X. Wu, J. Zhang, X. Ye, and Z. Qian, "Analysis and derivations for a family ZVS converter based on a new active clamp ZVS cell," *IEEE Trans. Ind. Electron.*, vol. 55, no. 2, pp. 773–781, Feb. 2008.
[2] R. G. Ganesan and M. Prabhakar, "Non-isolated high gain boost converter for photovoltaic applications," in *Proc. IEEE ICPEC*, 2013, pp. 277–280.
[3] L. S. Yang and T. J. Liang, "Analysis and implementation of a novel bidirectional DC-DC converter," *IEEE Trans. Ind. Electron.*, vol. 59, no. 1, pp. 422–434, Jan. 2012.
[4] C. T. Pan and C. M. Lai, "A high-efficiency high step-up converter with low switch voltage stress for fuel-cell system applications," *IEEE Trans. Ind. Electron.*, vol. 57, no. 6, pp. 1998–2006, Jun. 2010.
[5] H. M. Hsu and C. T. Chien, "Multiple turn ratios of on-chip transformer with four intertwining coils," *IEEE Trans. Electron Devices*, vol. 61, no. 1, pp. 44–47, Jan. 2014.
[6] X. Zhang *et al.*, "A wide bandgap device-based isolated quasi-switched-capacitor DC/DC converter," *IEEE Trans. Power Electron.*, vol. 29, no. 5, pp. 2500–2510, May 2014.
[7] B. Gu, J. Dominic, J. S. Lai, Z. Zhao, and C. Liu, "High boost ratio hybrid transformer DC-DC converter for photovoltaic module applications," *IEEE Trans. Power Electron.*, vol. 28, no. 4, pp. 2048–2058, Apr. 2013.
[8] H. S. Kim, J. W. Baek, M. H. Ryu, J. H. Kim, and J. H. Jung, "The high-efficiency isolated AC-DC converter using the three-phase interleaved LLC resonant converter employing the Y-connected rectifier," *IEEE Trans. Power Electron.*, vol. 29, no. 8, pp. 4017–4028, Aug. 2014.
[9] M. Sarhangzadeh, S. H. Hosseini, M. B. B. Sharifian, and G. B. Gharehpetian, "Multiinput direct DC-AC converter with high-frequency link for clean power-generation systems," *IEEE Trans. Power Electron.*, vol. 26, no. 6, pp. 1777–1789, Jun. 2011.
[10] P. H. Tseng, J. F. Chen, and Y. P. Hsieh, "A novel active clamp high step-up DC-DC converter with coupled-inductor for fuel cell system," in *Proc. IEEE IFEEC*, 2013, pp. 326–331.
[11] Y. H. Hu, W. D. Xiao, W. H. Li, and X. N. He, "Three-phase interleaved high-step-up converter with coupled-inductor-based voltage quadrupler," *IET Power Electron.*, vol. 7, no. 7, pp. 1841–1849, Jul. 2014.
[12] Y. Zhao, W. H. Li, and X. N. He, "Single-phase improved active clamp coupled-inductor-based converter with extended voltage doubler cell," *IEEE Trans. Power Electron.*, vol. 27, no. 6, pp. 2869–2878, Jun. 2012.
[13] T. Meng, S. Yu, H. Q. Ben, and G. Wei, "A family of multilevel passive clamp circuits with coupled inductor suitable for single-phase isolated full-bridge boost PFC converter," *IEEE Trans. Power Electron.*, vol. 29, no. 8, pp. 4348–4356, Aug. 2014.
[14] Y. P. Hsieh, J. F. Chen, T. J. Liang, and L. S. Yang, "Novel high step-up DC-DC converter with coupled-inductor and switched-capacitor techniques," *IEEE Trans. Ind. Electron.*, vol. 59, no. 2, pp. 998–1007, Feb. 2012.
[15] J. H. Lee, T. J. Liang, and J. F. Chen, "Isolated coupled-inductor-integrated DC-DC converter with nondissipative snubber for solar energy applications," *IEEE Trans. Ind. Electron.*, vol. 61, no. 7, pp. 3337–3348, Jul. 2014.
[16] J. Lei *et al.*, "A novel soft-switching bidirectional DC-DC converter with coupled inductors," in *Proc. IEEE APEC Expo.*, 2013, pp. 3040–3044.
[17] B. L. Narasimharaju, S. P. Dubey, and S. P. Singh, "Coupled inductor bidirectional DC-DC converter for improved performance," in *Proc. IEEE IECR*, 2010, pp. 28–33.
[18] F. Yang, X. B. Ruan, Q. Ji, and Z. H. Ye, "Input DM EMI filter design of interleaved CRM boost PFC converter with coupled inductor," in *Proc. IEEE ECCE*, 2011, pp. 2614–2621.
[19] T. J. Lin, J. F. Chen, and Y. P. Hsieh, "A novel high step-up DC-DC converter with coupled-inductor," in *Proc. IEEE IFEEC*, 2013, pp. 777–782.
[20] E. M. T. Miranda and R. P. B. Torrico, "An active clamping modified push-pull DC-DC converter," in *Proc. IEEE COBEP*, 2011, pp. 384–389.
[21] K. I. Hwu and Y. T. Yau, "High step-up converter based on coupling inductor and bootstrap capacitors with active clamping," *IEEE Trans. Power Electron.*, vol. 29, no. 6, pp. 2655–2660, Jun. 2014.
[22] K. C. Tseng, J. T. Lin, and C. A. Cheng, "An integrated derived boost-flyback converter for fuel cell hybrid electric vehicles," in *Proc. IEEE IFEEC*, 2013, pp. 283–287.
[23] S. M. Chen, C. Y. Wang, and T. J. Liang, "A novel sinusoidal boost-flyback CCM/DCM DC-DC converter," in *Proc. IEEE APEC Expo.*, 2014, pp. 3512–3516.
[24] J. Graw and H. Zimmermann, "Charging multiple batteries using the boost-flyback converter," in *Proc. IEEE ENERGYCON*, 2012, pp. 963–967.
[25] K. Umetani, S. Arimura, T. Hirano, J. Imaoka, and M. Yamamoto, "Evaluation of the Lagrangian method for deriving equivalent circuits of integrated magnetic components: A case study using the integrated winding coupled inductor," in *Proc. IEEE ECCE*, 2013, pp. 495–502.
[26] F. Yang, X. B. Ruan, Y. Yang, and Z. H. Ye, "Interleaved critical current mode boost PFC converter with coupled inductor," *IEEE Trans. Power Electron.*, vol. 26, no. 9, pp. 2404–2413, Sep. 2011.
[27] B. R. Lin and J. J. Chen, "Analysis and implementation of a soft switching converter with high-voltage conversion ratio," *IET Power Electron.*, vol. 1, no. 3, pp. 386–394, Sep. 2008.
[28] L. S. Yang, T. J. Liang, and J. F. Chen, "Transformerless DC-DC converters with high step-up voltage gain," *IEEE Trans. Ind. Electron*, vol. 56, no. 8, pp. 3144–3152, Aug. 2009.
[29] Y. Axelrod Berkovich and A. Ioinovici, "Switched-capacitor/switched-inductor structures for getting transformerless hybrid DC-DC PWM converters," *IEEE Trans. Circuits Syst. I, Reg. Papers*, vol. 55, no. 2, pp. 687–696, Mar. 2008.

Yu Tang (M'09) received the B.S. and the Ph.D. degrees in electrical engineering from Nanjing University of Aeronautics and Astronautics (NUAA), Nanjing, China, in 2003 and 2008, respectively.

Since 2008, he has been with the Department of Electrical Engineering, NUAA, where he is currently an Associate Professor with the College of Automation Engineering. He has published more than 20 papers in journals and conference proceedings and holds two China patents. His research areas include power electronics in renewable energy generation.

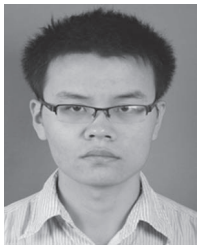

Dongjin Fu received the B.S. degree from the College of Electrical and Electronic Engineering, Shandong University of Technology, Zibo, China, in 2012. He is currently working toward the M.S. degree in the College of Automation Engineering, Nanjing University of Aeronautics and Astronautics, Nanjing, China.

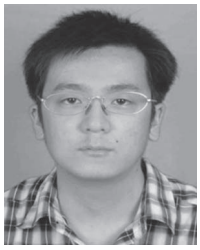

Ting Wang received the B.S. degree from the College of Electrical Engineering, Nantong University, Nantong, China, in 2011. He received the M.S. degree from the College of Automatic Engineering, Nanjing University of Aeronautics and Astronautics, Nanjing, China, in 2014.

He is currently an Application Engineer with DELAT, Inc.

Zhiwei Xu is currently working toward the B.E. degree in the College of Automation Engineering, Nanjing University of Aeronautics and Astronautics, Nanjing, China.